

Moments of Interference in Vehicular Networks with Hardcore Headway Distance

Konstantinos Koufos and Carl P. Dettmann

Abstract—Interference statistics in vehicular networks have long been studied using the Poisson Point Process (PPP) for the locations of vehicles. In roads with few number of lanes and restricted overtaking, this model becomes unrealistic because it assumes that the vehicles can come arbitrarily close to each other. In this paper, we model the headway distance (the distance between the head of a vehicle and the head of its follower) equal to the sum of a constant hardcore distance and an exponentially distributed random variable. We study the mean, the variance and the skewness of interference at the origin with this deployment model. Even though the pair correlation function becomes complicated, we devise simple formulae to capture the impact of hardcore distance on the variance of interference in comparison with a PPP model of equal intensity. In addition, we study the extreme scenario where the interference originates from a lattice. We show how to relate the variance of interference due to a lattice to that of a PPP under Rayleigh fading.

Index Terms—Headway models, interference modeling, stochastic geometry, vehicular networks.

I. INTRODUCTION

Interference statistics in wireless networks with unknown locations of users have long been studied using stochastic geometry [1]. Due to its analytical tractability, the Poisson Point Process (PPP) is the most commonly employed model. A PPP with non-homogeneous intensity has been used to capture a variable intensity of users due to mobility [2], [3]. The distribution of interferers in cellular uplink with a single interferer per Voronoi cell has also been approximated by non-uniform PPP [4]. Superposition of independent PPPs of different intensities is applicable to heterogeneous cellular networks [5]. By definition, a PPP assumes that two points (or users) can come arbitrarily close to each other. This assumption may not be accurate due to physical constraints and/or medium access control. In this regard, determinantal point processes have been used to describe the deployment of real-world macro base stations [6], [7], and Matérn point processes to model the locations of active transmitters in carrier sensing multiple access wireless ad hoc networks [8], [9]. The point processes suggested in [2]–[9] were constructed to study either planar cellular networks or one-dimensional (1D) ad hoc networks without deployment constraints. Therefore they are not immediately tailored to describe the unique deployment features of vehicular networks.

Vehicular networks are expected to play a key role in improving traffic efficiency and safety in the near future [10],

K. Koufos and C.P. Dettmann are with the School of Mathematics, University of Bristol, BS8 1TW, Bristol, UK. {K.Koufos, Carl.Dettmann}@bristol.ac.uk

This work was supported by the EPSRC grant number EP/N002458/1 for the project Spatially Embedded Networks. All underlying data are provided in full within this paper.

[11]. Using a planar two-dimensional PPP to study their performance along orthogonal streets is not accurate in the high reliability regime [12]. An interference model for vehicular networks should naturally combine two spatial models; one for the road infrastructure and another for the locations of vehicles along each road.

The Manhattan Poisson Line Process has been a popular model for the road network, where the resulting blocks might be filled in with buildings to resemble urban districts. In cellular systems, it has been shown that a user traveling on a street experiences discontinuous interference at the intersections [13]. In the absence of buildings, the interference from other roads can be easily mapped to interference from own road with a non-uniform density of users [14], [15]. Recently, the Poisson Line Process has been used to model the random orientations of roads [16], [17]. In an ad hoc setting, the intensities of roads and users have conflicting effects: Increasing the intensity of roads (while keeping fixed the intensity of vehicles per road) increases the interference while, increasing the intensity of vehicles reduces the average link distance and improves coverage [16].

A common assumption in [12]–[17] is that the distribution of vehicles along a roadway follows the 1D PPP. Similar assumption has been adopted for performance analysis over higher layers, e.g., the study in [18] jointly optimizes the transmission range and the transmission probability for maximizing transport capacity in linear networks with random access. There are some studies, e.g. [15], [19] using Matérn processes to approximate the density of simultaneous transmissions under the repulsive nature of IEEE 802.11p. The parent density is still PPP. Finally, connectivity studies combining queueing theory with random geometric graphs often make a similar assumption for exponential distribution of inter-arrivals [20].

A great deal of transportation research since the early 1960's has recognized that the distribution of headway distance (the distance measured from the head of a vehicle to the head of its follower [21], or simply the inter-vehicle distance) is not exponential under all circumstances. Different models were proposed to approximate the distribution of headway, with the accuracy of a particular model being dependent on the traffic status [22]. Empirical studies revealed that the distribution of time headway (time difference between successive vehicles as they pass a point on the roadway [21]) is well-approximated by the log-normal Probability Distribution Function (PDF) under free flow [23], [24] and by the log-logistic PDF under congested flow [22]. Due to the mixed traffic conditions, Cowan has proposed not only single (exponential, shifted-exponential), but also mixed distribution models to describe the distribution of headways [25].

To the best of our knowledge, apart from the exponential distribution, other headway models have not been incorporated into the interference analysis of vehicular networks. In [26], the log-normal distribution along with the Fenton-Wilkinson method for approximating the distribution of multi-hop distances has been used to study the lifetime of a link. The randomness is due to the speed and headway, while fading and interference are neglected.

Given a fixed and constant 1D intensity of users (or vehicles), the PPP assumes that their locations are independent. Let us now consider a simple enhancement to the PPP, which assumes that the headway distance is equal to the sum of a constant hardcore (or tracking) distance and an exponentially distributed Random Variable (RV). The hardcore distance may model the average length of a vehicle plus a safety distance. Since the hardcore distance is assumed fixed and constant, the PDF of headways becomes shifted-exponential. The motivation for this paper is to investigate how the first three moments of interference distribution behave under the shifted-exponential model. For instance, due to the fact that the deployment of interferers becomes more regular, the predicted interference is expected to have lower variance as compared to that originated from a PPP of equal intensity.

The shifted-exponential distribution of headways, makes the locations of vehicles correlated. The associated Pair Correlation Function (PCF) has been studied in the context of radial distribution function for hard spheres in statistical mechanics, see for instance [27], [28], and it has a complex form. As we will discuss later, the complexity of higher-order correlation functions does not allow us to calculate many more interference moments or bound the Probability Generating Functional (PGFL) [30]. Deriving the first moments of interference can serve as an intermediate step before approximating its PDF with some simple function (with known Laplace transform) using, for instance, the method of moments. The contributions of this paper are:

- For small hardcore distance c as compared to the mean inter-vehicle distance λ^{-1} , we show that the variance of interference at the origin can be approximated by the variance of interference due to a PPP of equal intensity λ scaled with $e^{-\lambda c}$. This model allows getting a quick insight on the impact of tracking distance c on the variance under various traffic conditions. In addition, it shows that the distribution of interference becomes more concentrated around the mean in comparison with that due to a PPP of intensity λ .
- We illustrate that large cell sizes r_0 and tracking distances c , modeling driving with high speeds at motorways, are associated with more concentrated distributions of interference (less coefficient of variation) and also more symmetric distributions (less skewness) in comparison with the distributions associated with urban microcells.
- We study the variance of interference due to 1D infinite lattice to shed some light on the behavior of interference when the tracking distance becomes comparable to the mean inter-vehicle distance, approximating scenarios like flow of platoons of vehicles and traffic jams. We devise a simple, yet accurate, model approximating the variance



Fig. 1. The vehicles are modeled as identical impenetrable disks. The vehicles outside of the cell (red disks) generate interference to the base station (black square). The rest (blue disks) are paired with the base station. In the figure, the tracking distance is illustrated equal to the diameter of the disk.

under the assumptions of Rayleigh fading and small inter-point lattice distance as compared to the cell size.

The rest of the paper is organized as follows. In Section II, we present the system set-up. In Section III, we calculate the pair and higher-order correlations for the new deployment model. In Section IV, we calculate the mean, the variance and the skewness of interference. In Section V, we derive closed-form approximations for the variance. In Section VI, we study the extreme case where the interference originates from a lattice. In Section VII, we conclude the paper and discuss topics for future work.

II. SYSTEM MODEL

Let us assume that the headway distance has two components: A constant tracking distance $c > 0$ and a free component following an exponential RV with mean μ^{-1} . This model degenerates to the time headway model M2 proposed by Cowan [25], if all vehicles move with the same constant speed towards the same direction. We study interference at a single snapshot. The base station is located at the origin, and the vehicles located in the interval $[-r_0, r_0]$ are associated to the base station, not contributing to interference level. The rest of the vehicles generate interference, see Fig. 1.

While the performance evaluation of wireless cellular networks focuses mostly on the downlink coverage of a user, the uplink performance in emerging vehicular networks would be important too. Besides downlink transmissions for entertainment and infotainment services while on-board, uplink transmissions would be critical for traffic coordination, efficiency and safety. A valid study for the uplink should naturally incorporate power control, and the constraint that a single vehicle per antenna sector transmits at a time-frequency resource block, see [29]. Due to the complex form of the PCF, we leave this modeling details for future work. In this paper, we will get a preliminary insight into the impact of correlated user locations on the moments of interference in the uplink.

Noting that the transmission range can be far greater than the width of a road, one may argue that in roads with multiple lanes, the distribution of inter-vehicle distances mapped onto a single line may still resemble an exponential. In Fig. 2a, it is illustrated that for $\lambda c = 0.4$ the distribution of inter-vehicle distances starts to converge to that due to a PPP (of equivalent intensity) for more than eight lanes. On the other hand, for smaller values of λc , e.g., $\lambda c = 0.1$ in Fig. 2b, only four lanes might be enough to achieve quite good convergence. Given that the product λc is fixed, the choice of parameters λ, c does not impact the speed of convergence. We see that for

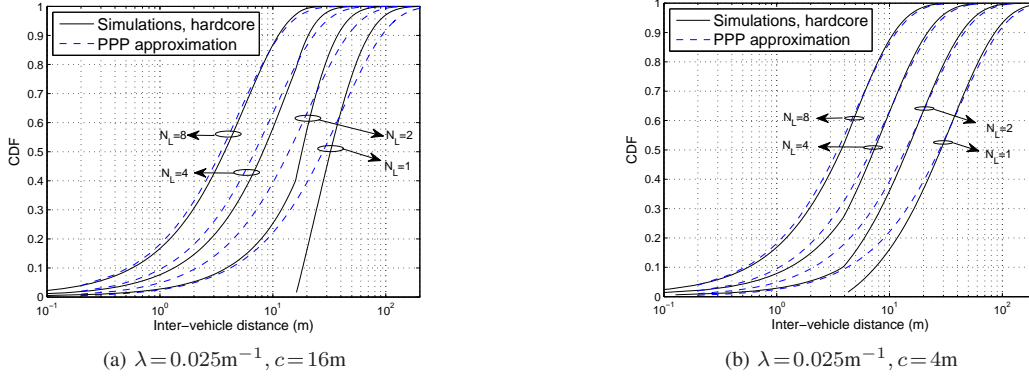


Fig. 2. Simulated CDF of inter-vehicle distances resulting from the independent superposition (on the same line) of N_L point processes of intensity λ and hardcore distance c . The approximating CDF using a PPP of equivalent intensity λN_L is $F(x) = 1 - e^{-\lambda N_L x}$. 10 000 simulation runs per curve.

two lanes, the sharp twist of the Cumulative Distribution Function (CDF) at inter-vehicle distance $x = c$ is still clear. Overall, the shifted-exponential model could be of use for roads with few lanes, e.g., bidirectional traffic streams with restricted overtaking. In this kind of scenario, the model helps avoid unrealistically small headway distances predicted by the PPP model with a high probability.

Regarding channel modeling, the propagation pathloss exponent is denoted by $\eta \geq 2$. The distance-based propagation pathloss function is $g(r) = |r|^{-\eta}$ for an interferer located at r with $|r| > r_0$, and zero otherwise, to filter out vehicles inside the cell. The fast fading over each link is Rayleigh, and its multiplicative impact h on the interference power is modeled by an exponential RV with mean unity, $\mathbb{E}\{h\} = 1$. The fading samples from different vehicles are independent and identically distributed (i.i.d.). The transmit power level is normalized to unity.

III. MOMENT MEASURES

The simplest function incorporating the distance-dependent constraints of a point process is the second-order intensity measure $\rho^{(2)}(x, y)$, or simply the PCF. It describes the joint probability there are two points in the infinitesimal regions dx, dy centered at x and y respectively. In order to express $\rho^{(2)}(x, y)$, we have to calculate the conditional probability there is a point at y given a point at x . For a PPP, the locations of different points are independent, thus $\rho^{(2)}(x, y) = \lambda^2$, where λ is the intensity. On the other hand, for the point process considered here the distance distribution between neighbors is shifted-exponential with positive shift c . Next, we show how to calculate $\rho^{(2)}(x, y)$ for this deployment rule. We will also generalize the calculation for the n -th order correlation function defined over n -tuples of points; needed in the calculation of the n -th moment of interference.

Due to the stationarity of the point process, the PCF depends on the distance separation between x and y . Let us assume $y > x > 0$ and denote by $\rho_k^{(2)}(y, x), k \in \mathbb{N}$, the branch of the PCF for $y \in (x + kc, x + (k+1)c)$. Since two vehicles are separated at least by the tracking distance, the PCF becomes zero for distances smaller than c , and thus $\rho_0^{(2)}(y, x) = 0$. For

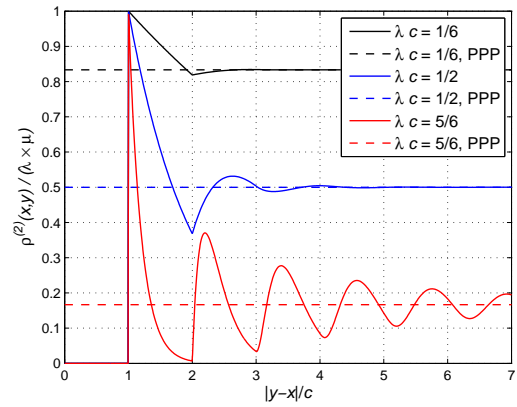


Fig. 3. Normalized PCF $\rho^{(2)}(x, y) / (\lambda\mu)$ with respect to the normalized distance $|y-x|/c$. The dashed lines correspond to $\rho^{(2)}(x, y) = \lambda^2$, or equivalently, $\rho^{(2)}(x, y) / (\lambda\mu) = 1 - \lambda c$.

distance separation between c and $2c$, no other vehicles can be located in-between. Therefore $\rho_1^{(2)}(y, x) = \lambda\mu e^{-\mu(y-x-c)}$, where $\lambda\mu dx dy$ is the probability that two vehicles are located in the infinitesimal regions dx, dy , and $e^{-\mu(y-x-c)}$ is the probability that no other vehicle is located in $(x+c, y)$. For distance separation between $2c$ and $3c$, at most one vehicle can be located in-between, and the PCF consists of two terms.

$$\begin{aligned} \rho_2^{(2)}(y, x) &= \frac{\lambda\mu}{e^{\mu(y-x-c)}} + \lambda \int_{x+c}^{y-c} \mu e^{-\mu(z-x-c)} \mu e^{-\mu(y-z-c)} dz \\ &= \frac{\lambda\mu}{e^{\mu(y-x-c)}} + \frac{\lambda\mu^2 (y-x-2c)}{e^{\mu(y-x-2c)}}, \end{aligned}$$

where $\mu e^{-\mu(z-x-c)} dz$ is the probability that a vehicle is located in the region dz centered at $z \in (x+c, y-c)$.

Following the same reasoning, when the distance $(y-x)$ is between $3c$ and $4c$, there are at most two vehicles in-between, and the PCF has three terms. The way to calculate the probabilities for zero and one vehicle between x and y has been shown. It remains to calculate the probability there are two vehicles. Let us assume that the vehicles are located at $z_1 < z_2$. Then $z_1 \in (x+c, y-2c)$ and $z_2 \in (z_1+c, y-c)$. The

probability that four vehicles are located at $x < z_1 < z_2 < y$ is

$$\lambda \int_{x+c}^{y-2c} \int_{z_1+c}^{y-c} \mu^3 e^{-\mu(z_1-x-c)} e^{-\mu(z_2-z_1-c)} e^{-\mu(y-z_2-c)} dz_2 dz_1.$$

After carrying out the integration and summing up,

$$\rho_3^{(2)}(y, x) = \frac{\lambda\mu}{e^{\mu(y-x-c)}} + \frac{\lambda\mu^2(y-x-2c)}{e^{\mu(y-x-2c)}} + \frac{\lambda\mu^3(y-x-3c)^2}{2e^{\mu(y-x-3c)}}.$$

Similarly, we can compute $\rho_k^{(2)}(y, x)$ for larger k .

$$\rho_k^{(2)}(y, x) = \begin{cases} \lambda \sum_{j=1}^k \frac{\mu^j (y-x-jc)^{j-1}}{\Gamma(j) e^{\mu(y-x-jc)}}, & y \in (x+kc, x+(k+1)c) \\ 0, & \text{otherwise,} \end{cases} \quad (1)$$

where $k \geq 1$ and $\Gamma(j) = (j-1)!$

Obviously, $\rho^{(2)}(x, y) = \sum_{k=0}^{\infty} \rho_k^{(2)}(y, x)$, $y > x$. For $y < x$, we just need to interchange x and y in (1). This PCF has also been studied in the context of statistical mechanics to describe the density variations of particles for 1D hardcore fluids as compared to the ideal (PPP) fluid [27], [28]. The derivation of (1) in [27], [28] is carried out using thermodynamic equations of state. It is the probability of finding a particle at a distance $(y-x)$ from an arbitrary fixed particle at x . We have used basic probability theory instead, to highlight the constraints introduced by the deployment rule. The Laplace transform of (1) is available in [31, pp. 5]. In Fig. 3, we depict the normalized PCF. For small λc , the function decorrelates within few multiples of c . For increasing λc , the locations of two vehicles can remain correlated over larger ranges.

Let us consider n points on the real line, x_1, x_2, \dots, x_n , in increasing order. According to [27, Eq. (27)], the higher-order intensity measure $\rho^{(n)}$, $n \geq 3$ for the shifted-exponential deployment has the following form, $\rho^{(n)}(x_1, x_2, \dots, x_n) = \frac{1}{\lambda^{n-2}} \prod_{i=1}^{n-1} \rho^{(2)}(x_{i+1} - x_i)$. For instance, the third-order intensity that describes the probability to find a triple of distinct vehicles at x, y and w , is

$$\rho^{(3)}(x, y, w) = \frac{1}{\lambda} \rho^{(2)}(x, y) \rho^{(2)}(y, w).$$

The performance assessment of wireless networks commonly utilizes the coverage probability as a metric, i.e., the probability (over the ensemble of all network states) that the Signal-to-Interference-and-Noise ratio is larger than a threshold. Even if the distribution of interference is unknown, the coverage probability could be computed, provided that the PGFL of the point process generating the interference is available. For a non-Poissonian point process, this is in general difficult to calculate. In addition, we saw that the n -th order intensity $\rho^{(n)}$ has increasing complexity for increasing n . Because of that, we could not simplify the multi-dimensional integrations in [30, Eq. (14)] to obtain tight bounds for the coverage probability. In order to bypass the calculation of the PGFL, we may approximate the interference by some well-known PDF with parameters, selected for instance using the method of moments. In that case, even two or three moments of interference might be sufficient for a good fit. Some discussion about the PDF of aggregate interference with a guard zone around the receiver can be found in [32, Section III]. In this regard, we show next how to calculate the first three moments of interference.

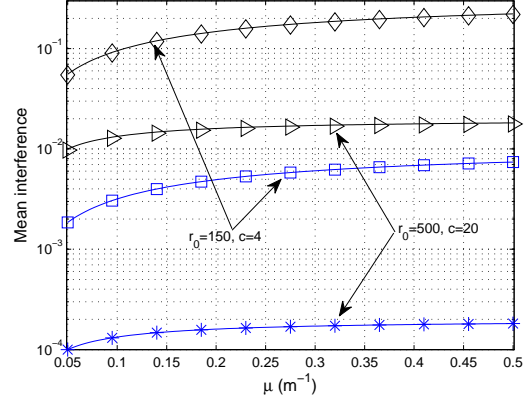


Fig. 4. Mean interference with respect to the random part μ of the intensity of vehicles. 50 000 simulation runs per marker over a line segment of 40 km. The solid lines correspond to (2) validated against the simulations (markers). Given the deployment scenario, the higher mean interference corresponds to pathloss exponent $\eta=2$, and the lower to $\eta=3$.

IV. MOMENTS OF INTERFERENCE

The mean interference at the origin can be calculated using the Campbell's Theorem for stationary processes [33]. Given the traffic parameters μ, c , the intensity λ of vehicles is constant and equal to $\lambda^{-1} = c + \mu^{-1}$, or $\lambda = \frac{\mu}{1+c\mu}$ [25]. After averaging the distance-based propagation pathloss over the intensity of interferers, we get the mean interference level.

$$\mathbb{E}\{\mathcal{I}\} = 2\lambda \mathbb{E}\{h\} \int_{r_0}^{\infty} g(r) dr = \frac{2\lambda r_0^{1-\eta}}{\eta-1}, \quad (2)$$

where the factor two is due to vehicles at negative half-axis.

In Fig. 4 we consider two scenarios: (i) tracking distance $c = 4$ m with cell size $r_0 = 150$ m modeling vehicular networks in urban street microcells, and (ii) $c = 20$ m and $r_0 = 500$ m modeling driving at higher speeds (hence the larger tracking distance) in motorway macrocells. We illustrate the mean interference for increasing traffic conditions, i.e., increasing the random part μ of the deployment model. For each scenario, we depict the interference level for two channel models, $\eta = 2$ and $\eta = 3$. The large cell size in conjunction with the large tracking distance makes the mean interference level less sensitive to the random part μ of the traffic intensity.

The mean interference due to a PPP of intensity λ is still given by (2). However, this is not the case for higher moments. We shall see that different hardcore distances c result in different variance and skewness of interference while keeping the intensity λ of vehicles fixed by varying $\mu = \frac{\lambda}{1-\lambda c}$.

The second moment of interference accepts contributions not only from a single vehicle but also from pairs.

$$\mathbb{E}\{\mathcal{I}^2\} = 2\lambda \int g^2(r) dr + \int g(x) g(y) \rho^{(2)}(x, y) dx dy, \quad (3)$$

where the factor two in front of the first term comes from the second moment of a unit-mean exponential RV, $\mathbb{E}\{h^2\} = 2$.

In order to calculate $S = \int g(x)g(y)\rho^{(2)}(x,y) dx dy$, we substitute equation (1) into it, remembering to interchange x and y for $x > y$.

$$\begin{aligned}
S &= 2 \sum_{k=1}^{\infty} \int_{r_0}^{\infty} \int_{x+kc}^{x+(k+1)c} g(x)g(y)\rho_k^{(2)}(y,x) dy dx + \\
&\quad 2 \sum_{k=1}^{\infty} \int_{r_0}^{\infty} \int_{x-(k+1)c}^{x-kc} g(x)g(y)\rho_k^{(2)}(x,y) dy dx \\
&= 2\lambda \sum_{k=1}^{\infty} \int_{r_0}^{\infty} \int_{x+kc}^{x+(k+1)c} g(x)g(y) \sum_{j=1}^k \frac{\mu^j (y-x-jc)^{j-1}}{\Gamma(j) e^{\mu(y-x-jc)}} dy dx + \\
&\quad 2\lambda \sum_{k=1}^{\infty} \int_{r_0}^{\infty} \int_{x-(k+1)c}^{x-kc} g(x)g(y) \sum_{j=1}^k \frac{\mu^j (x-y-jc)^{j-1}}{\Gamma(j) e^{\mu(x-y-jc)}} dy dx,
\end{aligned} \tag{4}$$

where the factor two is added to account for $x \leq -r_0$.

The calculation of S involves double integration, infinite sums and requires to filter out the vehicles within the cell. In order to simplify it, we note that for increasing distance separation, the PCF becomes progressively equal to λ^2 . Let us assume an integer $m \geq 2$, and approximate $\rho_k^{(2)}(y,x) \approx \lambda^2$, $\forall k \geq m$ (similar for $x > y$). From the first equality in (4) we have

$$\begin{aligned}
S &\approx 2 \sum_{k=1}^{m-1} \int_{r_0}^{\infty} \int_{x+kc}^{x+(k+1)c} g(x)g(y)\rho_k^{(2)}(y,x) dy dx + \\
&\quad 2 \sum_{k=1}^{m-1} \int_{r_0}^{\infty} \int_{x-(k+1)c}^{x-kc} g(x)g(y)\rho_k^{(2)}(x,y) dy dx + \\
&\quad 2\lambda^2 \sum_{k=m}^{\infty} \left(\int_{r_0}^{\infty} \int_{x+kc}^{x+(k+1)c} g(x)g(y) dy dx + \int_{r_0}^{\infty} \int_{x-(k+1)c}^{x-kc} g(x)g(y) dy dx \right).
\end{aligned}$$

The last line above can also be written as

$$2\lambda^2 \left(\int_{r_0}^{\infty} \int_{x+mc}^{\infty} g(x)g(y) dy dx + \int_{r_0}^{\infty} \int_{-\infty}^{x-mc} g(x)g(y) dy dx \right).$$

Using the exact expression of the PCF up to $(m+1)$ comes at the cost of calculating the integrals $\int_{r_0}^{\infty} \int_{x+mc}^{x+(m+1)c} g(x)g(y)\rho_m^{(2)}(y,x) dy dx$. Therefore the higher the m is, the higher is the penalty for improving the accuracy. For $m=2$ we get

$$\begin{aligned}
S &\approx 2\lambda\mu \int_{r_0}^{\infty} \left(\int_{x+2c}^{x+2c} \frac{g(x)g(y)}{e^{\mu(y-x-c)}} dy + \int_{x+2c}^{x-c} \frac{g(x)g(y)}{e^{\mu(x-y-c)}} dy \right) dx + \\
&\quad 2\lambda^2 \int_{r_0}^{\infty} \left(\int_{x+2c}^{x+c} g(x)g(y) dy + \int_{-\infty}^{x-2c} g(x)g(y) dy \right) dx.
\end{aligned} \tag{5}$$

In order to see the complications in the calculation of higher interference moments, we show the calculation of the third moment, which accepts contributions from a single user, from pairs and from triples of users.

$$\begin{aligned}
\mathbb{E}\{\mathcal{I}^3\} &= 6\lambda \int g^3(r) dr + 6 \int g^2(x)g(y)\rho^{(2)}(x,y) dx dy + \\
&\quad \int g(x)g(y)g(w)\rho^{(3)}(x,y,w) dx dy dw,
\end{aligned} \tag{6}$$

where the factor six in the first term comes from the third moment of an exponential RV, $\mathbb{E}\{h^3\} = 6$, and the same factor in the second term comes from multiplying the second moment

of an exponential RV, $\mathbb{E}\{h^2\} = 2$, with the three possible ways to select a pair out of a triple of users.

We still approximate the PCF by λ^2 beyond $2c$. The term $S' = \int g^2(x)g(y)\rho^{(2)}(x,y) dx dy$ can be expressed similar to the term S in (5).

$$\begin{aligned}
S' &\approx 2\lambda\mu \int_{r_0}^{\infty} \left(\int_{x+c}^{x+2c} \frac{g^2(x)g(y)}{e^{\mu(y-x-c)}} dy + \int_{x-2c}^{x-c} \frac{g^2(x)g(y)}{e^{\mu(x-y-c)}} dy \right) dx + \\
&\quad 2\lambda^2 \int_{r_0}^{\infty} \left(\int_{x+2c}^{\infty} g^2(x)g(y) dy + \int_{-\infty}^{x-2c} g^2(x)g(y) dy \right) dx.
\end{aligned}$$

Calculating $S'' = \int g(x)g(y)g(w)\rho^{(3)}(x,y,w) dx dy dw$ is more tedious because the third-order correlation is equal to the product of PCFs, $\rho^{(3)}(x,y,w) = \frac{1}{\lambda^3} \rho^{(2)}(x,y)\rho^{(2)}(y,w)$. Fortunately, the pathloss function $g(\cdot)$ is common for the three users. Therefore it suffices to calculate S'' for a particular order and scale the result by six.

$$\begin{aligned}
S'' &\approx \frac{6}{\lambda} \int g(x)g(y)g(w)\rho^{(2)}(x,y)\rho^{(2)}(y,w) dx dy dw + \\
&\quad 6\lambda \int g(x) dx \int g(y)g(w)\rho^{(2)}(y,w) dy dw,
\end{aligned}$$

where the first term corresponds to ordered users $x < y < w$ at the same side of the cell, and the second term describes the case with the user x (approximately) uncorrelated to the locations of y, w ($y < w$) because it is placed at the opposite side, thus $\rho^{(2)}(x,y) \approx \lambda^2$.

Since we consider the exact expression for the PCF up to $2c$, the first term of S'' above, let us denote it by S''_1 , can be separated into four terms describing the distance separations (closer or further than $2c$) between the users of each pair $\{y, w\}$ and $\{x, y\}$.

$$\begin{aligned}
S''_1 &\approx 12\lambda^2 \int_{r_0}^{\infty} \int_{x+2c}^{\infty} \left(\int_{y+c}^{y+2c} \frac{\mu g(w) dw}{e^{\mu(w-y-c)}} + \int_{y+2c}^{\infty} \lambda g(w) dw \right) g(x)g(y) dy dx + \\
&\quad 12\lambda\mu \int_{r_0}^{\infty} \int_{x+c}^{x+2c} \left(\int_{y+c}^{y+2c} \frac{\mu g(w) dw}{e^{\mu(w-y-c)}} + \int_{y+2c}^{\infty} \lambda g(w) dw \right) \frac{g(x)g(y)}{e^{\mu(y-x-c)}} dy dx,
\end{aligned}$$

where the factor two is due to symmetry, i.e., the three users are located at the negative half-axis.

We continue with the second term of S'' , let us denote it by S''_2 . In the expression of S''_2 the users y and w are already ordered and placed at the same side of the cell. After using the approximation for the PCF beyond $2c$ we get

$$\begin{aligned}
S''_2 &\approx 12\lambda^2 \int_{r_0}^{\infty} g(x) dx \left(\lambda \int_{r_0}^{\infty} \int_{y+2c}^{\infty} g(y)g(w) dw dy + \right. \\
&\quad \left. \mu \int_{r_0}^{\infty} \int_{y+c}^{y+2c} \frac{g(y)g(w) dw dy}{e^{\mu(w-y-c)}} \right),
\end{aligned}$$

where the factor two is again due to symmetry, i.e., the sides (with respect to the cell) of the user x and of the pair $\{y, z\}$ are interchanged.

In Fig. 5, we depict the coefficient of variation and the skewness of interference for two scenarios; urban ($c = 4$ m, $r_0 = 150$ m) and motorway ($c = 20$ m, $r_0 = 500$ m) cells. We calculate the standard deviation as $\sqrt{\mathbb{E}\{\mathcal{I}^2\} - \mathbb{E}\{\mathcal{I}\}^2}$, and

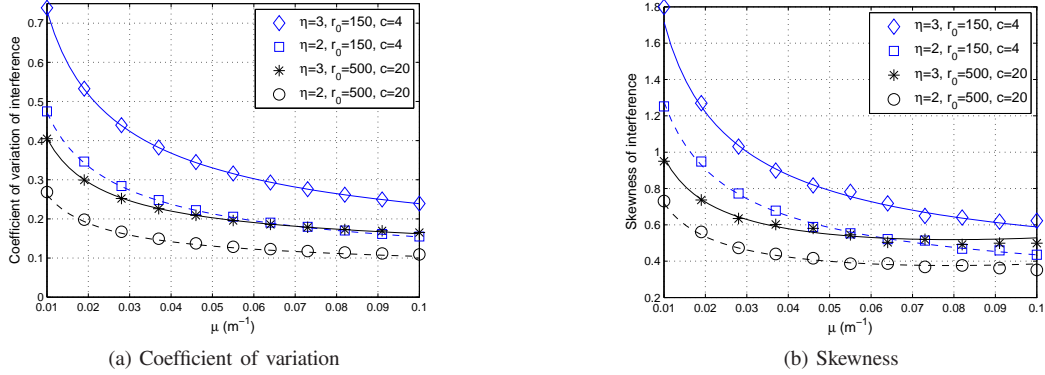


Fig. 5. Statistics of interference with respect to the random part μ of the deployment. The approximations (solid and dashed lines) use $m=2$ and numerical integration for the terms S, S', S''_1, S''_2 . The approximations are validated against the simulations (markers). 10^5 simulation runs per marker. The simulations are carried out over a line segment of 40 km.

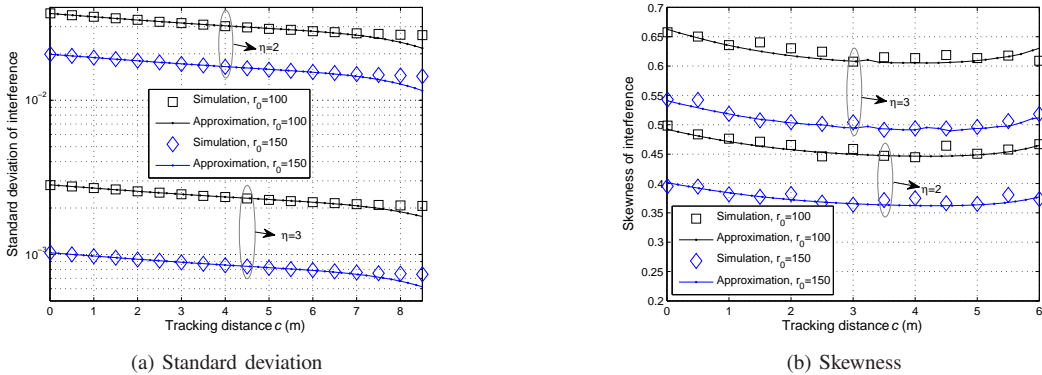


Fig. 6. Statistics of interference for a fixed intensity of vehicles $\lambda = 0.1\text{m}^{-1}$. The calculations using integral-based approximation for S, S', S''_1, S''_2 for $m=2$ are validated against the simulations (markers). 10^5 simulation runs per marker. The simulations are carried out over a line segment of 40 km.

the skewness as $\frac{\mathbb{E}\{\mathcal{I}^3\} - 3\mathbb{E}\{\mathcal{I}\}\mathbb{E}\{\mathcal{I}^2\} + 2\mathbb{E}\{\mathcal{I}\}^3}{(\mathbb{E}\{\mathcal{I}^2\} - \mathbb{E}\{\mathcal{I}\}^2)^{3/2}}$, where the terms $\mathbb{E}\{\mathcal{I}^2\}, \mathbb{E}\{\mathcal{I}^3\}$ in (3) and (6) are evaluated numerically using the approximations for the terms S, S', S'' with $m=2$. We depict the results up to $\mu = 0.1\text{m}^{-1}$. For $c = 20\text{m}$ and $\mu = 0.1\text{m}^{-1}$, we have $\lambda c = \frac{2}{3}$. For larger μ , the approximation accuracy with $m=2$ is poor in the motorway scenario because of long-range correlations. The mean and the variance of interference increase for a lower pathloss exponent given all other parameters remain fixed. We see in Fig. 5 that the coefficient of variation, defined as the ratio of the standard deviation over the mean, becomes smaller. Lower pathloss exponents are associated not only with more concentrated but also with more symmetric, less skewed, interference distributions. Given the pathloss model, the large cell size and tracking distance associated with the motorway scenario have the same effect on the distribution of interference. The distribution becomes more concentrated around the mean and also more symmetric between the tails in comparison with the interference distribution associated with urban microcells.

In Fig. 6 we have simulated the standard deviation and the skewness of interference with respect to the tracking distance c , while the intensity of vehicles λ is fixed. We have used cell sizes, $r_0 = 100\text{ m}$ and $r_0 = 150\text{ m}$, and pathloss exponents,

$\eta=2$ and $\eta=3$. We see that the approximations for the PCFs introduce negligible errors for $\lambda c \leq 0.6$. The approximation for the skewness is more prone to errors because the third moment consists of many terms involving the PCF and also, one term with the product of PCFs.

Based on Fig. 5 and Fig. 6 we deduce that the Gaussian model for the interference distribution would not be accurate in our system set-up. The distribution is skewed. This is in accordance with the study in [34], illustrating that a two-dimensional PPP with a guard zone around the receiver generates a positively skewed PDF for the aggregate interference under independent log-normal shadowing. We see in Fig. 6 that larger tracking distances make the variance of interference less for a fixed intensity of vehicles. This is intuitive because the deployment becomes more regular. The behaviour of the skewness does not appear to be monotonic.

The approximations we got so far do not provide much insight into the behaviour of second and third moment of interference, due to the complex nature of S, S', S'' . We would like to capture the impact of tracking distance on the moments of interference using a simple expression. Assuming an intensity λ of vehicles, how do the moments due to a hardcore process, $c > 0$, scale as compared to the respective moments due to a PPP of equal intensity λ ? Next, we assume,

in addition, a small tracking distance c as compared to the cell size r_0 . Under small λc and $\frac{c}{r_0}$, we will relate the standard deviation of interference to that due to a PPP, and draw useful remarks. The more complicated study about the behaviour of skewness, and the selection of appropriate models to describe the PDF of interference are left for future work.

V. CLOSED-FORM APPROXIMATION FOR THE VARIANCE

The contribution to the second moment of interference due to pairs of vehicles at distances larger than $2c$ is given by the second term in equation (5). Let us denote it by $S_{>2c}$. After substituting the propagation pathloss function we get

$$\begin{aligned} S_{>2c} &= 2\lambda^2 \left(\int_{r_0 x+2c}^{\infty} \int_{-\infty}^{\infty} x^{-\eta} y^{-\eta} dy dx + \int_{r_0}^{\infty} \int_{-\infty}^{x-2c} x^{-\eta} g(y) dy dx \right) \\ &\stackrel{(a)}{=} \frac{1}{2} \mathbb{E}\{\mathcal{I}\}^2 + 2\lambda^2 \left(\int_{r_0 x+2c}^{\infty} \int_{-\infty}^{\infty} \frac{dy dx}{x^\eta y^\eta} + \int_{r_0+2c}^{\infty} \int_{-\infty}^{x-2c} \frac{dy dx}{x^\eta y^\eta} \right) \\ &\stackrel{(b)}{=} \frac{1}{2} \mathbb{E}\{\mathcal{I}\}^2 + 4\lambda^2 \int_{r_0}^{\infty} \int_{-\infty}^{x+2c} x^{-\eta} y^{-\eta} dy dx \\ &\stackrel{(c)}{=} \frac{1}{2} \mathbb{E}\{\mathcal{I}\}^2 + \frac{2\lambda^2 r_0^{2-2\eta}}{\eta-1} \left(\frac{(2b+1)^{1-\eta}}{\eta-1} + \frac{2b}{2\eta-1} {}_2F_1(\eta, 2\eta-1, 2\eta; -2b) \right), \end{aligned} \quad (7)$$

where (a) follows from $2\lambda^2 \int_{r_0}^{\infty} \int_{-\infty}^{-r_0} x^{-\eta} |y|^{-\eta} dy dx = \frac{1}{2} \mathbb{E}\{\mathcal{I}\}^2$, (b) from symmetry, in (c) we substitute $b = \frac{c}{r_0}$, and ${}_2F_1$ is the Gaussian hypergeometric function [35, pp. 556].

Let us denote by $S_{<2c}$ the first term of S in (5), i.e., the contribution to the second moment from pairs of vehicles at distance separation less than $2c$. Due to the common pathloss function g over the users, the contributions to $S_{<2c}$ for $y > x$ and $x < y$ are equal (for $c < r_0$), and thus

$$S_{<2c} = 4\lambda\mu \int_{r_0}^{\infty} \int_{x+c}^{x+2c} x^{-\eta} y^{-\eta} e^{-\mu(y-x-c)} dy dx. \quad (8)$$

After integrating in terms of y we have

$$S_{<2c} = \frac{4\lambda}{\mu^{-\eta}} \int_{r_0}^{\infty} \frac{\Gamma(1-\eta, (c+x)\mu) - \Gamma(1-\eta, (2c+x)\mu)}{x^\eta e^{-\mu(c+x)}} dx, \quad (9)$$

where $\Gamma(a, x) = \int_x^{\infty} \frac{t^{a-1}}{e^t} dt$ is the incomplete Gamma function.

We cannot express the above integral in terms of well-known functions. In order to approximate it, we expand the integrand around $\mu(x+c) \rightarrow \infty$. For a fixed λ and $c > 0$, we have $\mu = \frac{\lambda}{1-\lambda c} > \lambda$. In addition, $(x+c) > r_0$. Therefore the expansion should be valid for $\lambda r_0 \gg 1$, i.e., the average number of vehicles within the cell must be high. After expanding up to the first-order term and carrying out the integration we get

$$\begin{aligned} S_{<2c} &\approx \int_{r_0}^{\infty} \frac{4\lambda}{(x(x+c))^\eta} \left(\frac{1-e^{-c\mu}}{\mu} + \frac{\eta(e^{-c\mu}(1+c\mu)-1)}{\mu^2(x+c)} \right) dx \\ &= \frac{4\lambda(1-e^{-c\mu}) {}_2F_1\left(\eta, 2\eta-1, 2\eta, -\frac{c}{r_0}\right)}{(2\eta-1) r_0^{2\eta-1}} + \\ &\frac{2\lambda(e^{-c\mu}(1+c\mu)-1) {}_2F_1\left(2\eta, \eta+1, 2\eta+1, -\frac{c}{r_0}\right)}{\mu r_0^{2\eta}}. \end{aligned} \quad (10)$$

For positive λ , the relation $\lambda c = 1$ corresponds to a lattice with inter-point distance $c = \lambda^{-1}$, and the relation $\lambda c = 0$ corresponds to a PPP of intensity λ . We would like to approximate the variance of interference for small c , while λ remains fixed. We start from the approximation of the term $S_{<2c}$ in (10), we substitute $\mu = \frac{\lambda}{1-\lambda c}$, and expand around $\lambda c \rightarrow 0$, up to second-order.

$$S_{<2c} \approx 2\lambda^2 c^2 \left(\frac{2r_0^{1-2\eta} {}_2F_1\left(2\eta-1, \eta, 2\eta, -\frac{c}{r_0}\right)}{(2\eta-1)c} - \frac{r_0^{-2\eta}}{2} {}_2F_1\left(2\eta, \eta+1, 2\eta+1, -\frac{c}{r_0}\right) \right). \quad (11)$$

After substituting (5) into (3), noting that $S = S_{>2c} + S_{<2c}$, carrying out the integration describing the contribution to the second moment from a single vehicle, we get

$$\text{Var}\{\mathcal{I}\} \approx \frac{4\lambda r_0^{1-2\eta}}{2\eta-1} + S_{>2c} + S_{<2c} - \mathbb{E}\{\mathcal{I}\}^2. \quad (12)$$

Next, we substitute (7) and (11) in (12).

$$\begin{aligned} \text{Var}\{\mathcal{I}\} &\approx \frac{4\lambda r_0^{1-2\eta}}{2\eta-1} + \frac{2\lambda^2 r_0^{2-2\eta}}{\eta-1} \left(\frac{(2b+1)^{1-\eta}}{\eta-1} + \frac{2b {}_2F_1(\eta, 2\eta-1, 2\eta; -2b)}{2\eta-1} \right) - \frac{\mathbb{E}\{\mathcal{I}\}^2}{2} + 2\lambda^2 r_0^{2-2\eta} \times \\ &\left(\frac{2b {}_2F_1(2\eta-1, \eta, 2\eta; -b)}{2\eta-1} - \frac{b^2 {}_2F_1(2\eta, \eta+1, 2\eta+1, -b)}{2} \right). \end{aligned}$$

After expanding up to second order in $b \rightarrow 0$ we have

$$\text{Var}\{\mathcal{I}\} \approx \frac{4\lambda r_0^{1-2\eta}}{2\eta-1} (1-\lambda c) + \lambda^2 c^2 r_0^{-2\eta}. \quad (13)$$

If we approximate the PCF one step further ($m=3$ instead of $m=2$), and repeat the same procedure, we end up with

$$\text{Var}\{\mathcal{I}\} \approx \frac{4\lambda r_0^{1-2\eta}}{2\eta-1} \left(1 - \lambda c + \frac{\lambda^2 c^2}{2} \right) + \lambda^2 c^2 r_0^{-2\eta}. \quad (14)$$

The leading order term, $r_0^{1-2\eta}$, in (13) and (14), will dominate the variance for $r_0 \gg c$. In addition, for small λc , we can use the expansion of the exponential function around zero, $e^{-\lambda c} \approx 1 - \lambda c + \frac{\lambda^2 c^2}{2}$, to get

$$\text{Var}\{\mathcal{I}\} \approx \frac{4\lambda r_0^{1-2\eta}}{2\eta-1} e^{-\lambda c}. \quad (15)$$

The above approximation relates in a simple manner the variance of interference due to a PPP of intensity λ , with the variance of interference due to a hardcore process of equal intensity, for small λc . Introducing a tracking distance c , while keeping the intensity λ fixed, makes the deployment more regular, and this results in exponential reduction $e^{-\lambda c}$ for the variance of interference, or equivalently, $e^{-\frac{\lambda c}{2}}$, for the standard deviation. The linear reduction (in logarithmic scale) of the standard deviation with respect to c is evident in Fig. 6. Using the approximation for the variance in (15), the coefficient of variation can be read as $\frac{\eta-1}{\sqrt{2\eta-1}} \frac{1}{\sqrt{\lambda r_0}} e^{-\frac{\lambda c}{2}}$. This approximation for the correlation coefficient agrees with the illustrations by Fig. 5a, and allows us to draw the following conclusion: The distribution of interference becomes more concentrated around

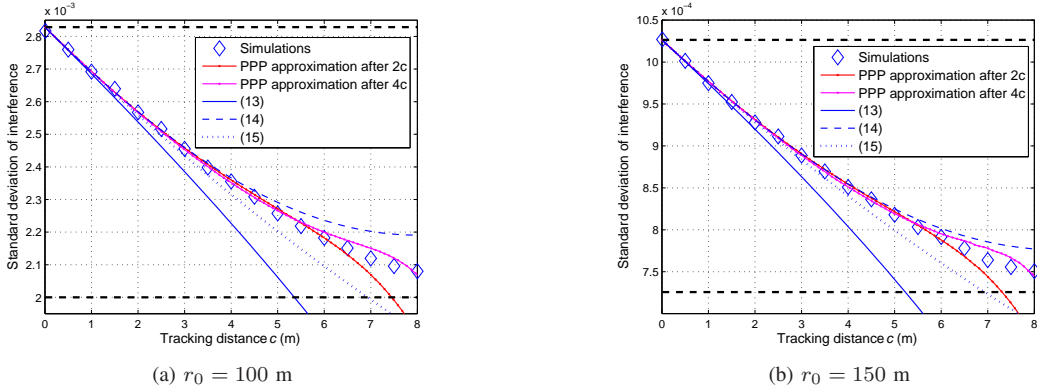


Fig. 7. Standard deviation of interference with respect to the tracking distance. The intensity is $\lambda = 0.1\text{m}^{-1}$. 2×10^5 simulation runs per marker. Pathloss exponent $\eta = 3$. For the 'PPP approximation after $2c$ ' we calculate $S_{>2c}$ from (7), and $S_{<2c}$ numerically from (8). In the numerical calculation of 'PPP approximation after $4c$ ', similar (but more) integrals to (7) and (8) are involved. The dashed line at the top corresponds to a PPP of intensity λ . The dashed line at the bottom corresponds to a lattice with inter-point distance λ^{-1} . The details for the calculation of the variance due to a lattice are given in Section VI.

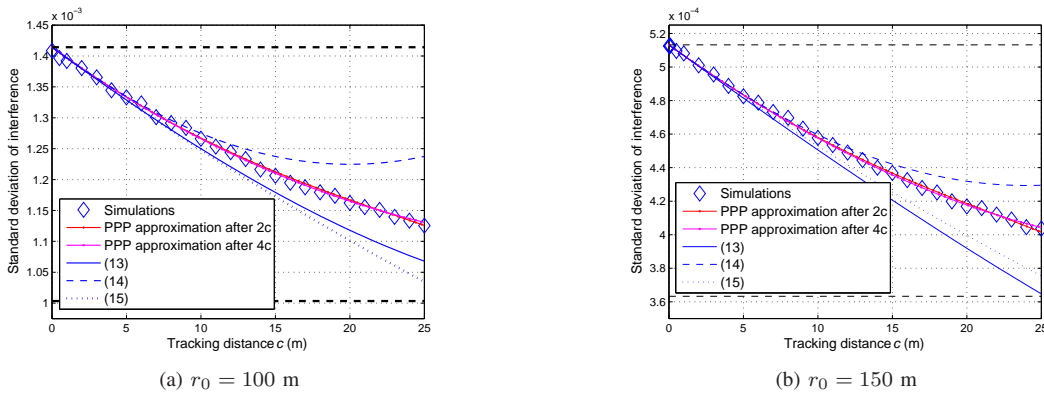


Fig. 8. Standard deviation of interference with respect to the tracking distance c . The intensity of vehicles is $\lambda = 0.025\text{m}^{-1}$. See the caption of Fig. 7 for parameter settings and explanation of the legends.

the mean for smaller pathloss exponent η , larger cell size r_0 , and increasing hardcore distance c while λ remains fixed.

In Fig. 7, we have simulated the standard deviation of interference for high traffic conditions $\lambda = 0.1\text{m}^{-1}$, i.e., on average one vehicle per 10 m. We depict the results for $\lambda c \in (0, 0.8)$. We see that the closed-form models (13)–(15) are indeed valid for small c . The model in (14) provides a good fit also for realistic tracking distances. This is because it uses the exact PCF up to $3c$ instead of $2c$. The considered distances, $c \in (0, 8)$ m are much smaller than the cell size r_0 , thereby the expansions around $b \rightarrow 0$ are accurate too. For tracking distances $c > 6$ m, the model using the exact PCF only up to $2c$ starts to fail, because of larger range correlations.

In Fig. 8, we replicate the results of Fig. 7 for lower traffic intensity, on average, one vehicle per 40 m. The average inter-vehicle distance becomes comparable to the cell size r_0 , and the feasible tracking distances span a much larger range. We depict the results up to $c = 25$ m, or equivalently $\lambda c \in (0, 0.625)$. We deduce that the models (13)–(15) do not fail due to the approximation of the PCF. We also note that the source of error is the approximation in $b \rightarrow 0$ rather than the expansion around $\lambda c \rightarrow 0$. The models (13)–(15) are still valid for small tracking distances c . For realistic values of c ,

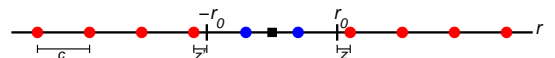


Fig. 9. One-dimensional lattice. The base station, 'black square', is located at the origin. Interference is due to points outside of the cell, 'red disks'. The RVs z, z' represent distances between the cell border and the lattice point nearest to it generating interference.

they give much more accurate predictions than the PPP.

VI. INTERFERENCE DUE TO A LATTICE

In the previous section, we constructed simple closed-form models for the variance of interference due to a hardcore process. These models fail to describe the variance with long-range correlations, i.e., $\lambda c \rightarrow 1$. Due to its high complexity, we leave this study for future, and study the extreme scenario, $\lambda c = 1$, to get a preliminary insight. For $\lambda c = 1$, the locations of vehicles form a lattice. Studying the moments of interference due to infinite lattices is also a preliminary step before incorporating more complicated deployments in our

analysis, e.g., Cowan M3 [25]. According to this model, finite lattices of geometrically distributed sizes are separated by exponentially distributed gaps, modeling bunches of vehicles with gaps in-between the bunches.

The performance of lattice networks (not only 1D) has been studied in [36]. Over there, the location of the receiver associated to the transmitter at the origin is optimized to maximize the achievable rate. Given the receiver's location, the interference from all points $\mathbb{Z} \setminus \{o\}$ becomes deterministic. In our system set-up, the sources of randomness are the Rayleigh fading and the distance z between the cell border r_0 and the nearest point to it generating interference, see Fig. 9. Since we know the locations of all interferers given $z \in (0, c)$, the PCF becomes an infinite series of Dirac delta functions, and this will greatly simplify the derivation of higher-order moments. For instance, we will show that the double integration $\int g(x)g(y)\rho^{(2)}(x,y)dxdy$ in the calculation of second moment degenerates to single integration in terms of z . The instantaneous interference at the base station due to the lattice points located at the positive half-axis is

$$\mathcal{I} = \sum_{k=0}^{\infty} h_k g(x_k) = \sum_{k=0}^{\infty} h_k g(r_0 + z + kc),$$

where h_k, x_k are the fading coefficient and location for the k -th point respectively, and z is a uniform RV, $z = U(0, c)$. The Moment Generating Function (MGF) of interference is

$$\Phi_{\mathcal{I}}(s) = \int e^{s\mathcal{I}} f_h f_x dh dx,$$

where h, x are the vectors of fading coefficients and user locations respectively, and f_h, f_x are the associated PDFs.

The mean interference can be calculated by evaluating the first derivative of the MGF at $s=0$.

$$\begin{aligned} \mathbb{E}\{\mathcal{I}\} &= \left. \frac{\partial \Phi_{\mathcal{I}}}{\partial s} \right|_{s=0} = 2 \int \sum_{k=0}^{\infty} h_k g(x_k) f_h f_x dh dx \\ &\stackrel{(a)}{=} 2 \int \sum_{k=0}^{\infty} h_k g(r_0 + z + kc) f_h f_z dh dz \\ &\stackrel{(b)}{=} 2 \int \sum_{k=0}^{\infty} g(r_0 + z + kc) f_z dz \\ &= \frac{2}{c} \int_0^c \sum_{k=0}^{\infty} (r_0 + z + kc)^{-\eta} dz \\ &= \frac{2}{c^{1+\eta}} \int_0^c \zeta\left(\eta, \frac{r_0 + z}{c}\right) dz, \end{aligned} \quad (16)$$

where the factor two has been added to account for lattice points in the negative half-axis, (a) is due to the fact that given z , the locations of all points become nonrandom, (b) follows from independent fading coefficients and $\mathbb{E}\{h_k\} = 1$, and $\zeta(n, x) = \sum_{k=0}^{\infty} (k+x)^{-n}$ is the Hurwitz Zeta function. After carrying out the integration in (16),

$$\mathbb{E}\{\mathcal{I}\} = \frac{2(\zeta(\eta-1, q) - \zeta(\eta-1, 1+q))}{c^\eta(\eta-1)} \stackrel{(a)}{=} \frac{2r_0^{1-\eta}}{c(\eta-1)}, \quad (17)$$

where $q = \frac{r_0}{c}$, and in (a) we have used the identity for consecutive neighbors $\zeta(n, x) = \zeta(n, 1+x) + x^{-n}$.

Due to the Campbell's Theorem [33], the mean interference can also be calculated by averaging the distance-based pathloss over the intensity of lattice points $\mathbb{E}\{\mathcal{I}\} = 2\lambda \int_0^\infty (r+r_0)^{-\eta} dr = \frac{2\lambda r_0^{1-\eta}}{\eta-1}$, where the intensity $\lambda = c^{-1}$.

In order to calculate the second moment of interference, we need to consider explicitly the interference originated from the negative half-axis. For that we have to identify the conditional Probability Mass Function (PMF) of the distance z' between the cell border $-r_0$ and the nearest lattice point to it generating interference, given the distance z , see Fig. 9. Let us denote $\epsilon = \frac{2r_0}{c} - \lfloor \frac{2r_0}{c} \rfloor$. The conditional PMF becomes equal to $z' = (c(1-\epsilon) - z)$ with probability $(1-\epsilon)$, and equal to $z' = (c(2-\epsilon) - z)$ with probability ϵ . For presentation clarity, we will assume that the diameter of the cell, $2r_0$, is an integer multiple of the inter-point distance, i.e., $\epsilon = 0$. In that case, $z' = (c - z)$ with probability one. Extensions and numerical results for a positive ϵ will be given.

The second moment of interference can be calculated by evaluating the second derivative of the MGF at $s=0$.

$$\begin{aligned} \mathbb{E}\{\mathcal{I}^2\} &= \left. \frac{\partial^2 \Phi_{\mathcal{I}}}{\partial s^2} \right|_{s=0} \\ &= \int \left(\sum_{k=0}^{\infty} h_k g(x_k) + \sum_{m=0}^{\infty} h_m g(x_m) \right)^2 f_h f_x dh dx \\ &= \int \left(2 \left(\sum_{k=0}^{\infty} h_k g(x_k) \right)^2 + 2 \sum_{k,m} h_k h_m g(x_k) g(x_m) \right) f_h f_x dh dx, \end{aligned}$$

where the sum over m describes the interference from the negative half-axis, and the factor two in front of the square term is due to symmetry.

After expanding the square term we have

$$\begin{aligned} \mathbb{E}\{\mathcal{I}^2\} &= \int \left(2 \left(\sum_{k=0}^{\infty} h_k^2 g(x_k)^2 + \sum_{k=0}^{\infty} \sum_{k' \neq k} h_k h_{k'} g(x_k) g(x_{k'}) \right) + \right. \\ &\quad \left. 2 \sum_{k=0}^{\infty} \sum_{m=0}^{\infty} h_k h_m g(x_k) g(x_m) f_h f_x \right) dh dx \\ &\stackrel{(a)}{=} \int \left(2 \left(\sum_{k=0}^{\infty} 2g(x_k)^2 + \sum_{k=0}^{\infty} \sum_{k' \neq k} g(x_k) g(x_{k'}) \right) + \right. \\ &\quad \left. 2 \sum_{k=0}^{\infty} \sum_{m=0}^{\infty} g(x_k) g(x_m) \right) f_x dx \\ &\stackrel{(b)}{=} \underbrace{2 \int \sum_{k=0}^{\infty} g(x_k)^2 f_x dx}_{J_1} + \underbrace{2 \int \sum_{k=0}^{\infty} \sum_{k' \neq 0} g(x_k) g(x_{k'}) f_x dx}_{J_2} + \\ &\quad \underbrace{2 \int \sum_{k=0}^{\infty} \sum_{m=0}^{\infty} g(x_k) g(x_m) f_x dx}_{J_3}, \end{aligned}$$

where (a) is due to $\mathbb{E}\{h_k^2\} = 2$, $\mathbb{E}\{h_k\} = 1$, and independent fading among the users, and in (b) we have added $k' = k$ in the second sum (so that the sum over k' goes over all positive integers similar to k) and subtract it from the first sum.

The distances z, z' to the cell borders are in general unequal $z \neq z'$. Therefore $J_2 \neq J_3$ (k' goes over the positive half- while m spans the negative half-axis). The term J_1 can be calculated

as in equation (17), i.e., conditioning in terms of z , integrating the Zeta function and using its consecutive neighbors identity

$$\begin{aligned} J_1 &= 2 \int \sum_{k=0}^{\infty} g(r_0+z+kc)^2 f_z dz \\ &= \frac{2}{c} \int_0^c \sum_{k=0}^{\infty} (r_0+z+kc)^{-2\eta} dz \\ &= \frac{2(\zeta(2\eta-1, q) - \zeta(2\eta-1, 1+q))}{c^{2\eta}(2\eta-1)} = \frac{2\lambda r_0^{1-2\eta}}{2\eta-1}. \end{aligned} \quad (18)$$

In a similar manner, the terms J_2 and J_3 can be expressed as

$$\begin{aligned} J_2 &= \frac{2}{c} \int_0^c \sum_{k=0}^{\infty} \sum_{k'=0}^{\infty} (r_0+z+kc)^{-\eta} (r_0+z+k'c)^{-\eta} dz \\ &= 2c^{-2\eta-1} \int_0^c \zeta\left(\eta, \frac{r_0+z}{c}\right)^2 dz. \\ J_3 &= \frac{2}{c} \int_0^c \sum_{k=0}^{\infty} \sum_{m=0}^{\infty} (r_0+z+kc)^{-\eta} (r_0+c-z+mc)^{-\eta} dz \\ &= 2c^{-2\eta-1} \int_0^c \zeta\left(\eta, \frac{r_0+z}{c}\right) \zeta\left(\eta, \frac{r_0+c-z}{c}\right) dz. \end{aligned} \quad (19)$$

For positive ϵ , the calculation of J_1 , J_2 and J_3 requires to average over the PMF of z' . The terms J_1 and J_2 would also include integrals of sums over the negative half-axis; instead of scaling by two the corresponding integrals over the positive half-axis. Due to the fact that the RV z' is also uniform, $z' = U(0, c)$, the terms J_1 and J_2 for $\epsilon > 0$ ends up equal to equations (18) and (19). The term J_3 contains the cross-terms, over the two axes, thus it requires to average over the PMF of the RV z' given z . The term J_3 for $\epsilon > 0$ will be larger than that in (19), reflecting the extra randomness introduced by the conditional PMF. Recall that for an arbitrary ϵ , $z' = ((1-\epsilon)c - z)$ for $z \leq (1-\epsilon)c$ and $z' = ((2-\epsilon)c - z)$ for $z > (1-\epsilon)c$. Therefore the term J_3 becomes

$$\begin{aligned} J_3 &= \frac{2}{c^{2\eta+1}} \int_0^{(1-\epsilon)c} \zeta\left(\eta, \frac{r_0+z}{c}\right) \zeta\left(\eta, \frac{r_0+c(1-\epsilon)-z}{c}\right) dz + \\ &\quad \frac{2}{c^{2\eta+1}} \int_{(1-\epsilon)c}^c \zeta\left(\eta, \frac{r_0+z}{c}\right) \zeta\left(\eta, \frac{r_0+c(2-\epsilon)-z}{c}\right) dz. \end{aligned} \quad (20)$$

For $\epsilon=0$, equation (20) degenerates to the expression of J_3 in (19). Finally, the variance of interference can be read as

$$\text{Var}\{\mathcal{I}\} = \frac{2\lambda r_0^{1-2\eta}}{2\eta-1} + J_2 + J_3 - \left(\frac{2\lambda r_0^{1-\eta}}{\eta-1}\right)^2. \quad (21)$$

In Fig. 10, the integral-based calculation of the variance, see (21) with the term J_3 calculated in (20), is verified with the simulations. We include also the calculations with the term J_3 calculated in (19), i.e., $\epsilon=0 \forall \{c, r_0\}$. The impact of positive ϵ becomes more prominent for higher inter-point distance c while keeping the cell size r_0 fixed.

The terms J_2 , J_3 are difficult to express in closed-form, see [37] for some recent work involving integrals of products of Zeta functions. A high precision evaluation of the Hurwitz Zeta function is also an issue because the function is an infinite sum [38]. In order to derive a closed-form approximation

for (21), we note that for large $q = \frac{r_0}{c}$, $\epsilon = 0$ and Rayleigh fading, the variance of interference due to a lattice can be well-approximated by $\frac{2\lambda r_0^{1-2\eta}}{2\eta-1}$. This is because the variance due to a PPP under Rayleigh fading, $\frac{4\lambda r_0^{1-2\eta}}{2\eta-1}$, accepts equal contributions, $\frac{2\lambda r_0^{1-2\eta}}{2\eta-1}$, due to fading and due to random user locations. The variance of interference due to a lattice with inter-point distance much less than the cell radius should be random mostly due to the fading, i.e., $\frac{2\lambda r_0^{1-2\eta}}{2\eta-1}$. In Fig. 10, we see that the corresponding curve due to a PPP of intensity $\frac{\lambda}{2}$ essentially overlaps with the curve depicting the integration-based results for a lattice with $c = \lambda^{-1}$ and $\epsilon = 0$. Their difference (not possible to notice it in the figure) is the standard deviation of interference due to a lattice without fading.

It might be useful to derive a closed-form approximation for the difference of the variances for $\epsilon > 0$ and $\epsilon = 0$. We recall it is only the term J_3 that depends on ϵ . Therefore we will expand J_3 for large q in (19) and (20), and take their difference. With large q , the argument of the Zeta function becomes also large, thus it can be well-approximated by an integral instead of a sum. Starting from (19) we get

$$\begin{aligned} J_3 &= 2c^{-2\eta} \int_0^1 \zeta(\eta, q+x) \zeta(\eta, q+1-x) dx \\ &\approx 2c^{-2\eta} \int_0^1 \left(\int_0^{\infty} (k+q+x)^{-\eta} dk \int_0^{\infty} (k+q+1-x)^{-\eta} dk \right) dx \\ &= \frac{2c^{-2\eta}}{(\eta-1)^2} \int_0^1 (q+x)^{1-\eta} (q+1-x)^{1-\eta} dx. \end{aligned}$$

For $q \gg x$, we may do first-order expansion.

$$\begin{aligned} J_3 &\approx \frac{2c^{-2\eta}}{(\eta-1)^2} \int_0^1 \left(q^{1-\eta} - \frac{(\eta-1)x}{q^\eta} \right) \left(q^{1-\eta} - \frac{(\eta-1)(1-x)}{q^\eta} \right) dx \\ &= \frac{r_0^{-2\eta} \left(c^2 (\eta-1)^2 - 6c(\eta-1)r_0 + 6r_0^2 \right)}{3c^2 (\eta-1)^2}. \end{aligned}$$

After approximating in a similar manner the term J_3 in (20) and subtract it from the above, we end up with $\epsilon(\epsilon-1)r_0^{-2\eta}$. Therefore the variance of interference due to a lattice of inter-point distance c can be approximated as

$$\text{Var}\{\mathcal{I}\} \approx \frac{2r_0^{1-2\eta}}{c(2\eta-1)} + \epsilon(1-\epsilon)r_0^{-2\eta}, \quad (22)$$

where for $\epsilon=0$, the variance has been approximated by the variance due to a PPP of intensity $\frac{1}{2c}$.

The accuracy of (22) is illustrated in Fig. 10, where it essentially overlaps with the integration-based results. Using $\epsilon = \frac{1}{2}$ in (22) indicates that under Rayleigh fading and large cell size, a lattice of intensity $\lambda = c^{-1}$ can at most increase by $\frac{r_0^{-2\eta}}{4}$ the variance of interference due to a PPP of intensity $\frac{\lambda}{2}$. This approximation is also available in Fig. 10, 'dashed cyan' curve. In Fig. 7 and Fig. 8, the selected values of cell size, r_0 , and intensity λ result in $\epsilon=0$. We can also observe over there the approximately $\sqrt{2}$ -relation of the standard deviations of interference due to a PPP and due to a lattice of equal intensity under Rayleigh fading.

The third moment of interference originated from a lattice can be calculated in a similar manner. The calculation is more

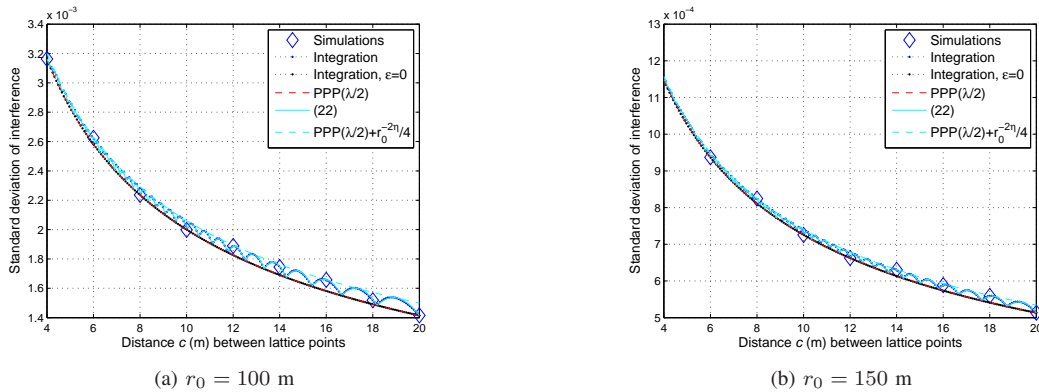


Fig. 10. Standard deviation of interference originated from a lattice. 5×10^6 simulation runs per marker. Pathloss exponent $\eta=3$. The integration corresponds to equation (21), where the terms J_2 in (19) and J_3 in (20) are evaluated numerically. The integration with $\epsilon=0$ calculates J_3 numerically from (19). The standard deviation of interference due to a PPP of intensity $\frac{\lambda}{2}$ is $\sqrt{\frac{2\lambda}{2\eta-1}r_0^{1-2\eta}}$, where $\lambda=c^{-1}$.

cumbersome because triples of sums are involved but it does not come with any new insights. The third-order correlation degenerates to one-dimensional integral with respect to z . A low-complexity approximation for the skewness, similar to the one in equation (22) for the variance, is also possible.

VII. CONCLUSIONS

In this paper we have shown that introducing small tracking distance c (as compared to the mean inter-vehicle distance λ^{-1}) in 1D vehicular networks reduces the variance of interference exponentially, $e^{-\lambda c}$, with respect to the variance due to a PPP of equal intensity λ . Since the mean interference levels under the two deployment models are equal, the coefficient of variation is reduced by $e^{-\frac{\lambda c}{2}}$, and the interference distribution becomes more concentrated around its mean. Assuming that the hardcore distance is fixed, the exponential correction makes sense to use especially under dense traffic, large λ . In addition, the distribution of interference for small λc remains positively-skewed, indicating that the gamma distribution would probably provide better fit than the normal distribution. We have also studied the extreme scenario where the interference originates from infinite 1D lattice to get some first insight into the properties of interference due to the flow of platoons of vehicles. Under Rayleigh fading and large cell size r_0 in comparison with the inter-point lattice distance c , we have shown that the term $\left(\frac{2r_0^{1-2\eta}}{c(2\eta-1)} + \frac{r_0^{-2\eta}}{4}\right)$ can be used as a tight upper bound for the variance of interference. The results of this paper can serve as a preliminary step before studying the probability of outage in the uplink of vehicular networks with a more realistic deployment model than the PPP. Temporal and spatial aspects of interference and more complex headway models are also relevant topics, the reader may refer to [39] for some recent results.

REFERENCES

- [1] M. Haenggi *et al.*, “Stochastic geometry and random graphs for the analysis and design of wireless networks”, *IEEE J. Sel. Areas Commun.*, vol. 27, pp. 1029-1046, Sept. 2009.
- [2] Z. Gong and M. Haenggi, “Interference and outage in mobile random networks: Expectation distribution and correlation”, *IEEE Trans. Mobile Comput.*, vol. 13, pp. 337-349, Feb. 2014.
- [3] K. Koufos and C.P. Dettmann, “Temporal correlation of interference and outage in mobile networks over one-dimensional finite regions”, *IEEE Trans. Mobile Comput.*, vol. 17, pp. 475-487, Feb. 2018.
- [4] M. Haenggi, “User point processes in cellular networks”, *IEEE Wireless Commun. Lett.*, vol. 6, pp. 258-261, Apr. 2017.
- [5] H.S. Dhillon, R.K. Ganti, F. Baccelli, and J.G. Andrews, “Modeling and analysis of K-tier downlink heterogeneous cellular networks”, *IEEE J. Sel. Areas Commun.*, vol. 30, pp. 550-560, Apr. 2012.
- [6] N. Miyoshi and T. Shirai, “A cellular network model with Ginibre configured base stations”, *J. Advances Appl. Probability*, vol. 46, pp. 832-845, 2014.
- [7] Y. Li, F. Baccelli, H.S. Dhillon, and J.G. Andrews, “Statistical modeling and probabilistic analysis of cellular networks with determinantal point processes”, *IEEE Trans. Commun.*, vol. 63, pp. 3405-3422, Sept. 2015.
- [8] A. Busson, G. Chelius and J.M. Gorce, “Interference modeling in CSMA multi-hop wireless networks”, [Research Report] RR-6624, INRIA, pp. 21, 2009.
- [9] M. Haenggi, “Mean interference in hard-core wireless networks”, *IEEE Commun. Lett.*, vol. 15, pp. 792-794, Aug. 2011.
- [10] 5G Automotive Association (5GAA), “The case for cellular V2X for safety and cooperative driving”, White Paper, Nov. 2016, available at <http://5gaa.org/wp-content/uploads/2017/10/5GAA-whitepaper-23-Nov-2016.pdf>
- [11] G. Karagiannis *et al.*, “Vehicular networking: A survey and tutorial on requirements, architectures, challenges, standards and solutions”, *IEEE Commun. Surveys and Tutorials*, vol. 13, no. 4, pp. 584-616, 2011.
- [12] J.P. Jeyaraj and M. Haenggi, “Reliability analysis of V2V communications on orthogonal street systems”, in *Proc. IEEE Globecom Workshops*, Singapore, 2017, pp. 1-6.
- [13] F. Baccelli and X. Zhang, “A correlated shadowing model for urban wireless networks”, in *Proc. IEEE Int. Conf. Comput. Commun. (INFOCOM)*, Hong Kong, 2015, pp. 801-809.
- [14] E. Steinmetz, M. Wildemeersch, T. Quek and H. Wymeersch, “A stochastic geometry model for vehicular communication near intersections”, in *Proc. IEEE Globecom Workshops*, San Diego, 2015, pp. 1-6.
- [15] M.J. Farooq, H. ElSawy and M.-S. Alouini, “A stochastic geometry model for multi-hop highway vehicular communication”, *IEEE Trans. Wireless Commun.*, vol. 15, pp. 2276-2291, Mar. 2016.
- [16] V.V. Chetlur and H.S. Dhillon, “Coverage analysis of a vehicular network modeled as Cox Process driven by Poisson Line Process”, *IEEE Trans. Wireless Commun.*, vol. 17, pp. 4401-4416, Jul. 2018.
- [17] C.-S. Choi and F. Baccelli, “An analytical framework for coverage in cellular networks leveraging vehicles”, *IEEE Trans. Commun.*, to be published.
- [18] B. Błaszczyszyn, P. Mühlethaler and Y. Toor, “Stochastic analysis of Aloha in vehicular ad hoc networks”, *Ann. of Telecommun.*, vol. 68, pp. 95-106, Feb. 2013.
- [19] Z. Tong H. Lu, M. Haenggi and C. Poellabauer, “A stochastic geometry approach to the modeling of DSRC for vehicular safety communication”, *IEEE Trans. Intell. Transp. Syst.*, vol. 17, pp. 1448-1458, May 2016.

- [20] N.P. Chandrasekharamenon and B. Ancharev, "Connectivity analysis of one-dimensional vehicular ad hoc networks in fading channels", *EURASIP J. Wireless Commun. and Networking*, Springer International Publishing, 2012.
- [21] Highway Capacity Manual, Transportation Research Board, National Research Council, Washington, DC, 2000.
- [22] S. Yin *et.al.*, "Headway distribution modeling with regard to traffic status", *IEEE Intell. Vehicles Symp.*, Xian, 2009, pp. 1057-1062.
- [23] A. Daou, "On flow within platoons", *Australian Road Research*, vol. 2, no. 7, pp. 4-13, 1966.
- [24] I. Greenberg, "The log-normal distribution of headways", *Australian Road Research*, vol. 2, no. 7, pp. 14-18, 1966.
- [25] R.J. Cowan, "Useful headway models", *Transportation Research*, vol. 9, no. 6, pp. 371-375, Dec. 1975.
- [26] G. Yan and S. Olariu, "A probabilistic analysis of link duration in vehicular ad hoc networks", *IEEE Trans. Intell. Transp. Syst.*, vol. 12, pp. 1227-1236, Dec. 2011.
- [27] Z.W. Salsburg, R.W. Zwanzig and J.G. Kirkwood, "Molecular distribution functions in a one-dimensional fluid", *J. Chemical Physics*, vol. 21, pp. 1098-1107, Jun. 1953.
- [28] R.L. Sells, C.W. Harris and E. Guth, "The pair distribution function for a one-dimensional gas", *J. Chemical Physics*, vol. 21, pp. 1422-1423, 1953.
- [29] T.D. Novlan, H.S. Dhillon and J.G. Andrews, "Analytical modeling of uplink cellular networks", *IEEE Trans. Wireless Commun.*, vol. 12, pp. 2669-2679, Jun. 2013.
- [30] R.K. Ganti, F. Baccelli and J.G. Andrews, "Series expansion for interference in wireless networks", *IEEE Trans. Inf. Theory*, vol. 58, pp. 2194-2205, Apr. 2012.
- [31] D.C. Mattis, The many-body problem. An Encyclopedia of exactly solved models in one dimension. World Scientific Publishing, 1993.
- [32] H. ElSawy, E. Hossain and M. Haenggi, "Stochastic geometry for modeling, analysis, and design of multi-tier and cognitive cellular wireless networks: A survey", *IEEE Commun. Surveys and Tutorials*, vol. 15, no. 3, pp. 996-1019, 2013.
- [33] S.N. Chiu, D. Stoyan, W.S. Kendall and J. Mecke, Stochastic geometry and its applications. ISBN: 978-0-470-66481-0, 2013.
- [34] A. Ghasemi and E.S. Sousa, "Interference aggregation in spectrum-sensing cognitive wireless networks", *IEEE J. Sel. Topics Signal Process.*, vol. 2, pp. 41-56, Feb. 2008.
- [35] M. Abramowitz and I.A. Stegun. Handbook of mathematical functions with formulas, graphs and mathematical tables. Washington, DC, USA: GPO, 1972.
- [36] M. Haenggi, "Interference in lattice networks", *available at* <https://arxiv.org/abs/1004.0027>, 2010.
- [37] M.A. Shpot, and R.B. Paris, "Integrals of products of Hurwitz zeta functions via Feynman parametrization and two double sums of Riemann zeta functions", *Mathematica Aeterna*, vol. 6, no. 5, pp. 745-764, 2016. Available at http://www.e-hilaris.com/MA_volume6.html
- [38] F. Johansson, "Rigorous high-precision computation of the Hurwitz zeta function and its derivatives", *Numerical Algorithms*, Springer US, vol. 69, no. 2, pp. 253-270, Jun. 2015.
- [39] K. Koufos and C.P. Dettmann, "Performance of a link in a field of vehicular interferers with hardcore headway distance", *submitted for publication*, available at <https://arxiv.org/abs/1810.00959>, 2018.